

# Parity-time symmetry and variable optical isolation in active-passive-coupled microresonators

Long Chang<sup>1,2</sup>, Xiaoshun Jiang<sup>1,2\*</sup>, Shiyue Hua<sup>1,2</sup>, Chao Yang<sup>1,2</sup>, Jianming Wen<sup>3\*</sup>, Liang Jiang<sup>3</sup>, Guanyu Li<sup>1,2</sup>, Guanzhong Wang<sup>1,2</sup> and Min Xiao<sup>1,2,4\*</sup>

**Compound-photonic structures with gain and loss<sup>1</sup> provide a powerful platform for testing various theoretical proposals on non-Hermitian parity-time-symmetric quantum mechanics<sup>2-5</sup> and initiate new possibilities for shaping optical beams and pulses beyond conservative structures. Such structures can be designed as optical analogues of complex parity-time-symmetric potentials with real spectra. However, the beam dynamics can exhibit unique features distinct from conservative systems due to non-trivial wave interference and phase-transition effects. Here, we experimentally realize parity-time-symmetric optics on a chip at the 1,550 nm wavelength in two directly coupled high-Q silica-microtoroid resonators with balanced effective gain and loss. With this composite system, we further implement switchable optical isolation with a non-reciprocal isolation ratio from  $-8$  dB to  $+8$  dB, by breaking time-reversal symmetry with gain-saturated nonlinearity in a large parameter-tunable space. Of importance, our scheme opens a door towards synthesizing novel micro-scale photonic structures for potential applications in optical isolators, on-chip light control and optical communications.**

One of the most fundamental postulates in canonical quantum mechanics, formulated by Dirac and von Neumann, mandates that the Hermiticity of each operator be directly associated with a physical observable. As such, the spectrum of a self-adjoint operator is ensured to be real and the total probability (or unitary evolution) is conserved. In 1998, however, Bender and colleagues<sup>2</sup> discovered a wide class of complex non-Hermitian Hamiltonians that can possess entirely real spectra below a certain phase-transition point, provided they satisfy combined parity-time (PT) symmetry. This counterintuitive discovery immediately aroused extensive theoretical interest in extending canonical quantum theory by including non-Hermitian but PT-symmetric operators<sup>2-5</sup>. For instance, a PT-symmetric Hamiltonian operator may contain a complex potential  $V(x)$  subject to a spatial-symmetry constraint  $V(x) = V^*(-x)$ . One of the most striking properties of a PT-symmetric operator stems from the appearance of a sharp, symmetry-breaking transition once a non-Hermitian operator crosses a certain critical threshold<sup>2-5</sup>. On crossing that 'exceptional point', the spectrum ceases to be real and starts to become complex. This transition signifies the appearance of a spontaneous PT symmetry breaking from the exact- to the broken-PT phase.

Despite much fundamental theoretical success in the development of PT-symmetric quantum mechanics, an experimental observation of pseudo-Hermiticity remains elusive and very challenging

in real physical settings. Thanks to the formal equivalence between the quantum-mechanical Schrödinger equation and the paraxial optical diffraction equation, complex PT-symmetric potentials can be easily achieved in optics by spatially modulating the refractive index with properly placed gain and loss in a balanced manner<sup>1</sup>. This analogy immediately spurred theoretical and experimental efforts in relation to PT symmetry using optics and other suitable physical systems. These include experimental set-ups with one optical component with absorption and another that is either optically pumped (active PT symmetry)<sup>6,7</sup> or lossless (passive PT symmetry)<sup>8</sup>. The PT phase transition has been studied in optical systems both theoretically<sup>9,10</sup> and experimentally<sup>6-8</sup>, and has been observed in non-Hermitian systems either with active PT symmetry composed of one amplifying and one attenuating LRC circuit<sup>11</sup> or in a dissipative microwave billiard<sup>12</sup>. Other suitable systems involving superconductors<sup>13</sup>, atomic gases<sup>14,15</sup> and plasmonics<sup>16</sup> have also been proposed theoretically. Further theoretical studies of PT symmetry-based effects reveal many interesting optical phenomena, including unconventional beam refraction<sup>17</sup>, conical diffraction<sup>18</sup>, unidirectional invisibility induced by PT-symmetric periodic structures<sup>19-21</sup> and coherent perfect laser absorption<sup>22,23</sup> (the latter two have been verified experimentally<sup>7,24,25</sup>).

Achieving rapid progress in integrated photonic circuits demands all-optical elements for high-speed processing of light signals. The optical isolator<sup>26</sup> is one such indispensable element. Similar to electronic diodes, it allows the flow of light to be unidirectional and reduces problems caused by unwanted reflections or interference effects. The successful design of an optical isolator relies on the breaking of time-reversal symmetry, as typically realized in magneto-optical media<sup>27</sup> through the inclusion of anti-symmetric off-diagonal dielectric tensor elements. Recently, unidirectional light reflection has been realized in PT-symmetric systems near the exceptional point, with reflection from one end being diminished, but amplified at the other end<sup>11,19-21,24</sup>. Inspired by these studies, we show another way to obtain tunable optical isolation in two coupled whispering-gallery-mode (WGM) microtoroids with gain and loss functionalities in a large parameter space. In contrast to previous results<sup>27-30</sup>, our system allows variable non-reciprocal transmissions<sup>31</sup>, even at very low light levels, by adjusting the coupling strengths or input laser power. Before illustrating the asymmetric light transport, we begin with PT symmetry in active-passive-coupled microcavities with balanced gain and loss. Remarkably, our scheme explicitly demonstrates itself to be an on-chip ultrasensitive optical isolator

<sup>1</sup>National Laboratory of Solid State Microstructures and College of Engineering and Applied Sciences, Nanjing University, Nanjing 210093, China,

<sup>2</sup>Synergetic Innovation Center in Quantum Information and Quantum Physics, Nanjing University, Nanjing 210093, China, <sup>3</sup>Department of Applied Physics, Yale University, New Haven, Connecticut 06511, USA, <sup>4</sup>Department of Physics, University of Arkansas, Fayetteville, Arkansas 72701, USA.

\*e-mail: jxs@nju.edu.cn; jianming.wen@yale.edu; mxiao@uark.edu

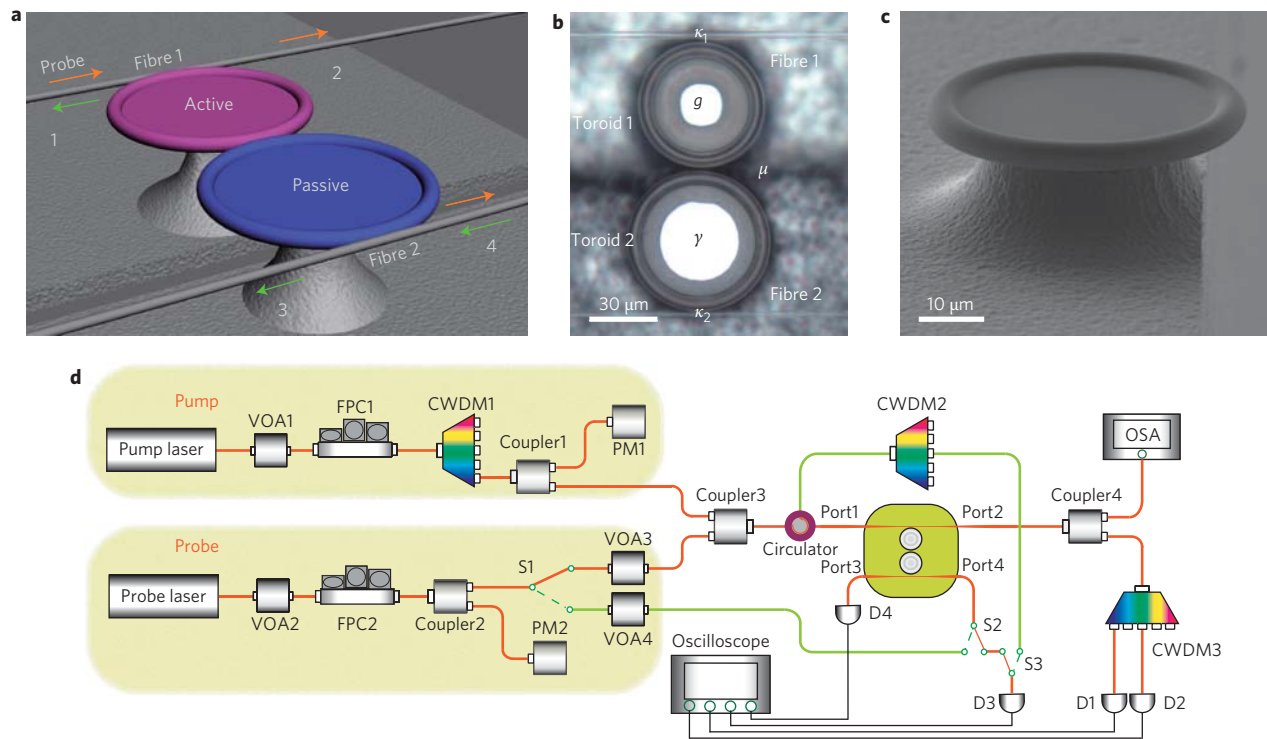


**Figure 1 | On-chip WGM silica microtoroid resonators with gain and loss for PT symmetry and optical isolation.** **a**, Schematic three-dimensional view of the system, which is composed of two directly coupled microtoroids coupled to two tapered fibres (1 and 2). Based on the probe input directions, forward and backward propagation configurations are denoted by orange and green arrows, respectively. **b**, Top-view optical microscope image of the system in **a**, where  $g$  represents the effective gain in active toroid 1,  $\gamma$  the total loss rate of passive toroid 2,  $\mu$  the coupling strength between the two toroids, and  $\kappa_1$  ( $\kappa_2$ ) the coupling strength between toroid 1 (2) and fibre 1 (2), respectively. **c**, Side-view scanning electron microscopy (SEM) image of the fabricated microtoroid cavity located at the edge of the silicon chip. **d**, Schematic of the experimental set-up. VOA, variable optical attenuator; FPC, fibre polarization controller; PM, power meter; CWDM, coarse wavelength division multiplexer; OSA, optical spectrum analyser.

(or circulator) with an isolation ratio of +8 dB at an input probe power of 11.4 nW. Its compatibility with conventional metal-oxide-semiconductor processing further makes this structure potentially useful for on-chip optical communications, computation and photonic switching.

Our system consists of two directly coupled active-passive silica microtoroids<sup>32</sup>, fabricated at the edges of silicon chips<sup>33,34</sup> (Fig. 1). The active microtoroid (labelled ‘toroid 1’) was fabricated from erbium-doped silica sol-gel film<sup>35,36</sup>, optically pumped by a 1,480 nm narrow-linewidth tunable laser to produce an effective gain ( $g = g'/2 - \gamma_{1/2} - \kappa_{1/2}$ , where  $g' = g_0/(1 + |a_1/a_{\text{sat}}|^2)$ ; see Supplementary Section I) in the 1,550 nm band (Fig. 2a,b). The passive toroid (labelled ‘toroid 2’) is a high-quality microresonator with decay rate  $\gamma$ . The two toroids are coupled to tapered optical fibres 1 and 2 (Fig. 1a,b), respectively. In the experiment, the two cavities are prepared to support similar initial resonance frequencies and the same polarization at 1,553 nm to coincide with the emission of erbium ions. The pump field only circulates in toroid 1 due to the mode mismatch between the two resonators at the pump wavelength. To accurately tune the coupling strengths of the toroid-toroid and tapered fibre-toroid, the microcavities and fibre tapers were all mounted on nanopositioning translation stages for precision controls of their separation distances. Also, each microtoroid was placed on an actively controlled thermoelectric cooler (TEC) element to stabilize (with a stability of <10 mK) and change the resonance frequency of the resonator. The intrinsic  $Q$ -factors of toroids 1 and 2 were measured to be  $5.75 \times 10^5$  and  $5.33 \times 10^6$ , respectively, at 1,553.0 nm, and the intrinsic  $Q$ -factor of toroid 1 at 1,478.7 nm was  $2.24 \times 10^6$ .

The PT-symmetric property was investigated under the balanced gain and loss ( $g = \gamma$ ) condition. After carefully balancing the gain and loss in the microtoroids (see Methods), the pump power was fixed and the transmitted probe spectra were studied as a function of the coupling strength  $\mu$  between the two microtoroids by changing the position of toroid 2 (Fig. 2c,d) while keeping the frequency detuning between the two microcavities fixed ( $\sim 0$ ). To start, we first blocked the pump laser to reduce the system to passively coupled microtoroids<sup>34</sup> (in which we can observe two supermodes<sup>34</sup> determined by  $\mu$  and the decay rates of the two resonators). Then, with the pump laser on, frequency bifurcation induced by PT symmetry exhibits distinct features in spectral location change and linewidth narrowing. In particular, a PT phase transition occurs at the critical point where  $\mu = \gamma = g$ . Theoretically (see Supplementary Section I), for  $\mu > \gamma$  the system is in the unbroken phase and two real spectral branches  $\omega_{\pm}$  with zero linewidth are displaced at  $\pm \sqrt{\mu^2 - \gamma^2}$  away from the central cavity-resonant frequency. When  $\mu < \gamma$ , the PT symmetry is spontaneously broken because  $\omega_{\pm}$  now take complex values. The experimental results (Fig. 2c,d) confirm the theory, and also demonstrate the vivid evolution of PT supermodes from the unbroken to broken phase as the separation distance between the two toroids is increased continuously. Significant signal amplification in the output (Fig. 2c) due to the spectral singularity of the complex optical potential also verifies the theoretical prediction by Mostafazadeh<sup>37</sup>. The doublet feature of each PT supermode in the transmission spectra (Fig. 2c) is a result of the mode splitting caused by the mode coupling between the clockwise and anticlockwise modes<sup>38,39</sup>. By taking into account this scattering-induced mode splitting in the theory, the

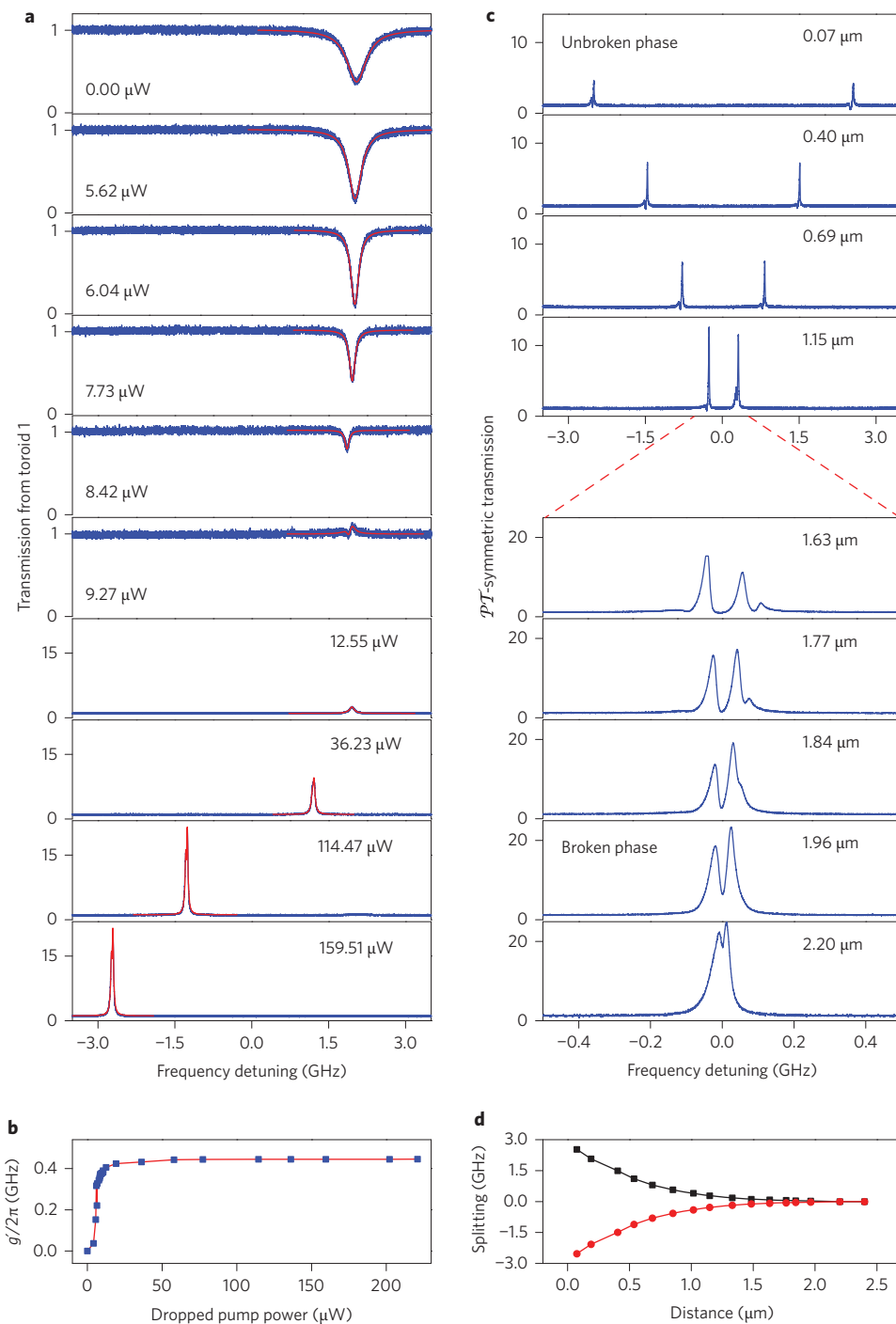


**Figure 2 | Transmission spectra in PT symmetry.** **a**, Transmission spectra of active toroid 1, obtained by altering the dropped pump power for a fixed probe power of 31.3 nW. **b**, Plot of gain  $g'$  in **a** as a function of dropped pump power. The data clearly exhibit the effect of gain saturation nonlinearity. **c**, Evolution of PT-symmetric transmission spectra measured at port 2 in the broken and unbroken phases, obtained by varying the coupling strength (or separation distance) of the two toroids. The input probe and dropped pump powers are fixed at 11.4 nW and 146.7  $\mu\text{W}$ , respectively. **d**, Spectral splitting between the two PT supermodes in **c** as a function of the separation distance between the two toroids.

experimental results can be well fitted with numerical simulations (Supplementary Fig. 2).

It is well known that a linear static dielectric system, even in the presence of gain and loss, cannot have a non-reciprocal response<sup>26</sup>. Previous studies have found that, with the addition of a Kerr-type nonlinearity<sup>40</sup>, the system may display very strong non-reciprocity. To break the reciprocal transmission in the linear PT-symmetric

regime we carried out a set of experiments on optical isolation (see Methods) by exploring the gain saturation-induced nonlinearity (existing in toroid 1) to smash the time-reversal symmetry. It turns out that the probe gain is very easily saturated when increasing the input probe and/or pump powers. In contrast to previous studies<sup>11,19–21,24,27–31</sup>, our system further exhibits a switchable isolation direction on elevating the incident probe power from a few

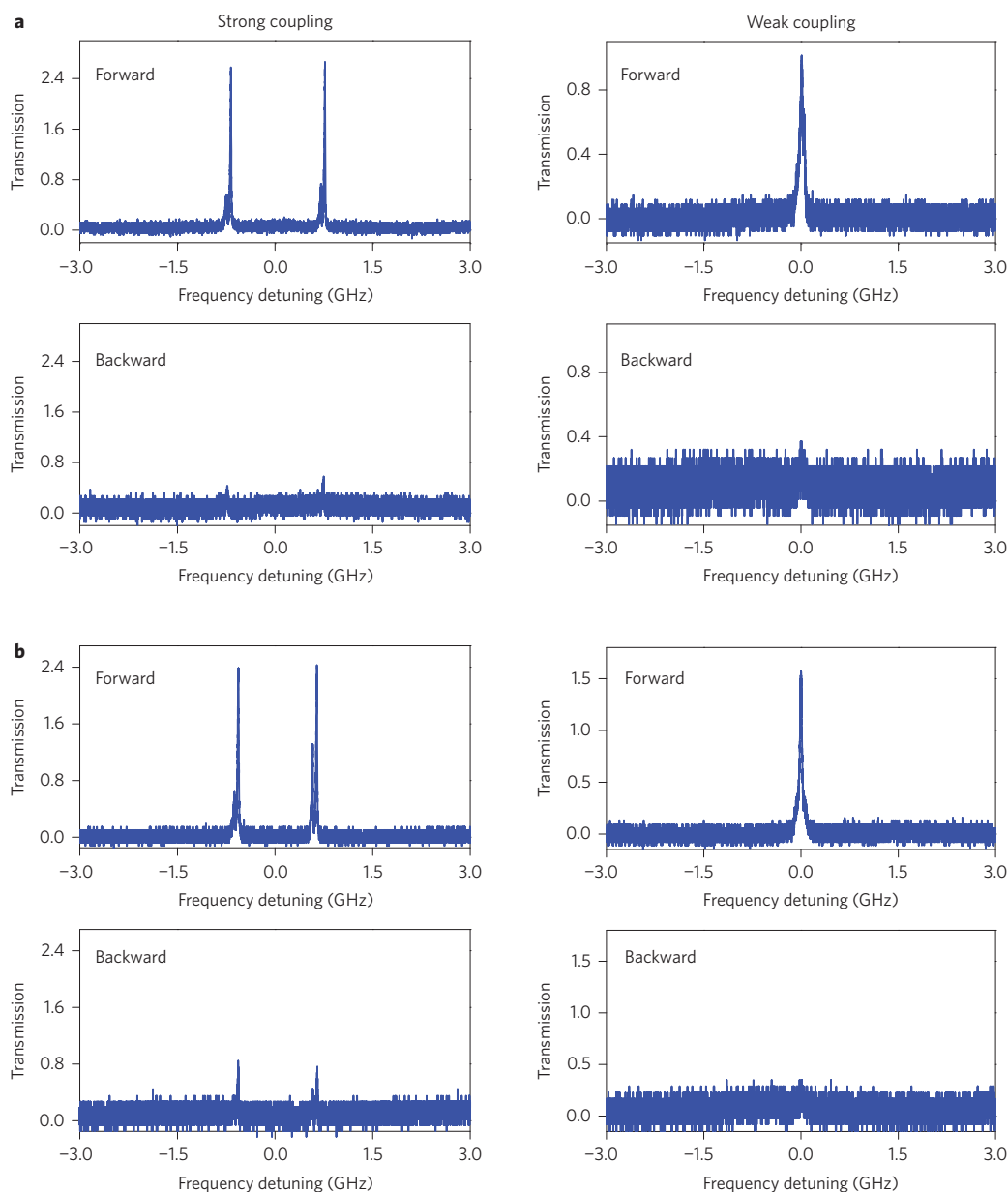


**Figure 3 | Supersensitive optical isolation performance of the system.** **a,b**, Representative optical isolation at a very low probe power (11.4 nW) but with different dropped pump powers (149.2  $\mu\text{W}$  and 192.9  $\mu\text{W}$ ). Non-reciprocal transmittance spectra are clearly demonstrated under both strong and weak coupling between the two microtoroids. In **a** and **b** the isolation ratios at strong and weak coupling regimes are (+7.8 dB, +5.8 dB) and (+5.4 dB, +7.5 dB), respectively.

nanowatts to  $\sim 30$   $\mu\text{W}$ . Experimentally, we achieved an isolation ratio, given by

$$10 \times \log_{10} \left( \frac{\text{maximal transmission in forward}}{\text{maximal transmission in backward}} \right)$$

ranging from +8 dB to  $-8$  dB. By engineering the coupling strengths ( $\mu$ ,  $\kappa_1$ ,  $\kappa_2$ ) and input pump power, the isolation ratio can also be altered in a controllable manner. For example, Fig. 3a,b presents snapshots of asymmetric transmission spectra obtained under the same input probe power (11.4 nW) but with different coupling strengths  $\mu$  and dropped pump powers. Specifically, Fig. 3a shows non-reciprocal forward–backward transport with a dropped pump power of 149.2  $\mu\text{W}$  and comparable gain

and loss ( $g \approx \gamma$ ). Under the strong coupling condition ( $\mu > g$ ,  $\gamma$ ), the mode-splitting feature can be clearly observed in both probe propagation configurations. In the weak coupling regime ( $\mu < g$ ,  $\gamma$ ), the splitting coalesces into a single mode. Similarly, these phenomena can be attained with a higher dropped pump power (192.9  $\mu\text{W}$ ; Fig. 3b). In Fig. 3a,b, the isolation ratios for strong and weak coupling cases are, respectively, (+7.8 dB, +5.8 dB) and (+5.4 dB, +7.5 dB). The presence of optical non-reciprocity at such a low probe power demonstrates the supersensitivity of the performance of the device. In comparison with the non-reciprocity achieved with two passive silicon microring cavities<sup>31</sup>, our scheme yields a good isolation performance due to gain-saturation-induced nonlinearity, even at the ultralow probe power of a few nanowatts, which is several orders of magnitude lower than that reported in ref. 31.

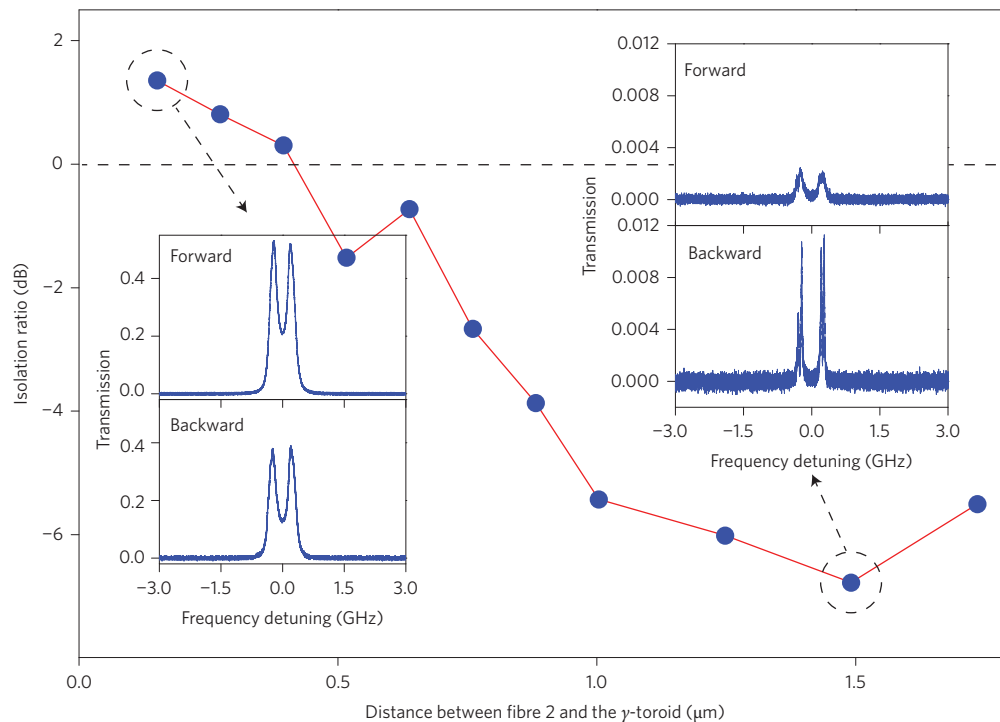


**Figure 4 | Optical isolation performance of the device versus separation distance between toroid 2 and fibre 2.** Experimental data clearly show the capability of controlling the device performance by tailoring the coupling strength  $\kappa_2$  between toroid 2 and fibre 2. The probe and dropped pump powers are 26  $\mu\text{W}$  and 140.1  $\mu\text{W}$ , respectively. Insets: snapshots showing non-reciprocal transmission spectra where the maximal isolation ratios are obtained in the forward and backward propagation configurations.

To further test the performance and controllability, we implemented measurements by only modifying the coupling strength  $\kappa_2$  between fibre 2 and toroid 2, with fixed input probe/pump powers and other coupling strengths ( $\mu$  and  $\kappa_1$ ). Apparently, a similar isolation behaviour is achieved, as shown in Fig. 4, where the probe power is maintained at  $\sim 26 \mu\text{W}$ . As one can see, when the coupling between fibre 2 and toroid 2 is weak, the isolation ratio takes a negative sign, which indicates more backward transmission than forward. However, when the coupling is large enough, the isolation ratio becomes positive, showing more output from the forward configuration. From Figs 2–4 it is worth noting that the use of a gain toroid allows the system to yield a narrower transmission linewidth than with only passive ones. In coupled-mode theory (see Supplementary Section II), our theoretical simulations can explain the observed phenomena well (Figs 3 and 4) by including the gain-saturation nonlinearity.

It is now evident that the present microscale optical structure with active-passive-coupled WGM microcavities is not only appropriate for studies of PT-symmetric optics, but is also suitable as an on-chip ultrasensitive, variable optical isolator with an isolation ratio ranging from  $-8 \text{ dB}$  to  $+8 \text{ dB}$  at the optical communications wavelength. By tuning the system parameters, the non-reciprocal direction can be easily reversed for potential application as an optical switch. From a device integration standpoint our design has the advantages of compact footprint and variable isolation ratio, which are important in making progress in the realization of on-chip photonic integration. As a fundamental building block to achieve on-chip optical non-reciprocity, this architecture demonstrates a wide operating scope for the probe power, ranging from a few nanowatts up to tens of microwatts. Furthermore, the introduction of gain-saturable nonlinearity may bring optical bistability (and multistability) within the PT symmetry framework and optical isolation. All these attributes deserve further investigation and encourage new discoveries of counter-intuitive optical phenomena as well as a new generation of PT-symmetric optical devices.

*Note added in proof:* During the review process we became aware of a recent paper by Peng and co-workers<sup>41</sup>, in which they also experimentally demonstrated PT symmetry and non-reciprocal light transmission in coupled WGM microcavities. The experimental demonstrations and the theoretical model used in the current work go beyond those described in ref. 41.

## Methods

**Balancing gain and loss.** In PT-symmetric optics, one key procedure is to approach the critical condition by balancing the gain and loss (that is,  $g = \gamma$ ). To achieve this necessary condition (Fig. 1b,d) we first brought the two WGM microtoroids close enough together to ensure that the coupling strength  $\mu$  was larger than  $g$  and  $\gamma$ . We then coupled toroid 1 with tapered fibre 1, but decoupled fibre 2 from toroid 2. After these two steps we gradually tuned the pump power until the probe transmission at port 2 was observed to reach its maximum for a fixed probe input power. At this point, the gain and loss were balanced. During the entire process, the pump detuning with the  $g$ -toroid resonant frequency shift and the temperature of the  $\gamma$ -cavity were well adjusted to compensate for the thermal effect arising from optical pumping<sup>42</sup>. It should be mentioned that to make the resonance frequencies of the two microcavities very close, we controlled the temperatures of the two microcavities to ensure that the splitting modes exhibited almost the same transmission.

**Optical isolation measurement.** Figure 1d presents a schematic diagram of the set-up for the optical isolation measurements. Two tunable narrow linewidth lasers, operating at 1,480 nm and 1,550 nm bands, were used as the pump and probe light sources, respectively. The optical powers and polarizations of both lasers were adjusted by variable optical attenuators (VOA1 and VOA2) and fibre polarization controllers (FPC1 and FPC2). Two optical couplers (coupler1 and coupler2) were used to monitor the pump and probe optical powers. Before entering coupler 1, the pump light passed through a coarse wavelength division multiplexer (CWDM1) to filter out noises at the 1,550 nm band. Three optical switches (S1, S2 and S3) were used to switch the paths of the probe light and measure the transmission difference between the forward and backward propagation configurations. For backward transmission measurements, the probe laser was launched into the coupled microcavities from port 4 by connecting two optical switches (S1 and S2) to a variable optical attenuator (VOA4). The dropped transmitted light from port 1 passed through an optical fibre circulator and a CWDM2 (to filter out the reflected pump light) connected to the third optical switch (S3). Two variable optical attenuators (VOA3 and VOA4) were used to balance the insertion losses between the forward and backward transmissions and to ensure that the optical powers of the

probe fields from both paths were equal. (In the experiment, the backward transmission has more insertion loss, so we add more additional optical loss using VOA3 to make the insertion losses the same in both transmission directions. In addition, VOA4 is needed because the variable optical attenuators have their own insertion losses.) These arrangements are very important, because the gain saturation in the active microtoroid is very sensitive to the circulated probe power. The third CWDM (CWDM 3) was used to separate the pump and probe light measured by detectors D1 and D2, respectively.

Received 28 January 2014; accepted 10 May 2014;  
published online 22 June 2014

## References

- El-Ganainy, R., Makris, K. G., Christodoulides, D. N. & Musslimani, Z. H. Theory of coupled optical PT-symmetric structures. *Opt. Lett.* **32**, 2632–2634 (2007).
- Bender, C. M. & Boettcher, S. Real spectra in non-Hermitian Hamiltonians having PT symmetry. *Phys. Rev. Lett.* **80**, 5243–5246 (1998).
- Bender, C. M., Boettcher, S. & Meisinger, P. N. PT-symmetric quantum mechanics. *J. Math. Phys.* **40**, 2201–2229 (1999).
- Bender, C. M. Making sense of non-Hermitian Hamiltonians. *Rep. Prog. Phys.* **70**, 947–1018 (2007).
- Mostafazadeh, A. Pseudo-Hermiticity versus PT symmetry: the necessary condition for the reality of the spectrum of a non-Hermitian Hamiltonian. *J. Math. Phys.* **43**, 205–214 (2002).
- Ruter, C. E. *et al.* Observation of parity–time symmetry in optics. *Nature Phys.* **6**, 192–195 (2010).
- Regensburger, A. *et al.* Parity–time synthetic photonic lattices. *Nature* **488**, 167–171 (2012).
- Guo, A. *et al.* Observation of PT-symmetry breaking in complex optical potentials. *Phys. Rev. Lett.* **103**, 093902 (2009).
- Berry, M. V. Optical lattices with PT symmetry are not transparent. *J. Phys. A* **41**, 244007 (2008).
- Klaيمان, S., Gunther, U. & Moiseyev, N. Visualization of branch points in PT-symmetric waveguides. *Phys. Rev. Lett.* **101**, 080402 (2008).
- Bender, N. *et al.* Observation of asymmetric transport in structures with active nonlinearities. *Phys. Rev. Lett.* **110**, 234101 (2013).
- Bittner, S. *et al.* PT symmetry and spontaneous symmetry breaking in a microwave billiard. *Phys. Rev. Lett.* **108**, 024101 (2012).
- Chtchelkatchev, N. M., Golubov, A. A., Baturina, T. I. & Vinokur, V. M. Stimulation of the fluctuation superconductivity by PT symmetry. *Phys. Rev. Lett.* **109**, 150405 (2012).
- Hang, C., Huang, G. & Konotop, V. V. PT symmetry with a system of three-level atoms. *Phys. Rev. Lett.* **110**, 083604 (2013).
- Sheng, J., Miri, M.-A., Christodoulides, D. N. & Xiao, M. PT-symmetric optical potentials in a coherent atomic medium. *Phys. Rev. A* **88**, 041803 (2013).
- Benisty, H. *et al.* Implementation of PT symmetric devices using plasmonics: principle and applications. *Opt. Express* **19**, 18004–18019 (2011).
- Makris, K. G., El-Ganainy, R., Christodoulides, D. N. & Musslimani, Z. H. Beam dynamics in PT symmetric optical lattices. *Phys. Rev. Lett.* **100**, 103904 (2008).
- Ramezani, H., Kottos, T., Kovanis, V. & Christodoulides, D. N. Exceptional-point dynamics in photonic honeycomb lattices with PT symmetry. *Phys. Rev. A* **85**, 013818 (2012).
- Lin, Z. *et al.* Unidirectional invisibility induced by PT-symmetric periodic structures. *Phys. Rev. Lett.* **106**, 213901 (2011).
- Longhi, S. Invisibility in PT-symmetric complex crystals. *J. Phys. A* **44**, 485302 (2011).
- Mostafazadeh, A. Invisibility and PT symmetry. *Phys. Rev. A* **87**, 012103 (2013).
- Longhi, S. PT-symmetric laser absorber. *Phys. Rev. A* **82**, 031801(R) (2010).
- Chong, Y. D., Ge, L. & Stone, A. D. PT-symmetry breaking and laser-absorber modes in optical scattering systems. *Phys. Rev. Lett.* **106**, 093902 (2011).
- Feng, L. *et al.* Experimental demonstration of a unidirectional reflectionless parity–time metamaterial at optical frequencies. *Nature Mater.* **12**, 108–113 (2013).
- Sun, Y., Tan, W., Li, H.-Q., Li, J. & Chen, H. Experimental demonstration of a coherent perfect absorber with PT phase transition. *Phys. Rev. Lett.* **112**, 143903 (2014).
- Jalas, D. *et al.* What is—and what is not—an optical isolator. *Nature Photon.* **7**, 579–582 (2013).
- Bi, L. *et al.* On-chip optical isolation in monolithically integrated non-reciprocal optical resonators. *Nature Photon.* **5**, 758–762 (2011).
- Gallo, K., Assanto, G., Parameswaran, K. R. & Fejer, M. M. All-optical diode in a periodically poled lithium niobate waveguide. *Appl. Phys. Lett.* **79**, 314–316 (2001).
- Sukhrukov, A. A., Xu, Z. Y. & Kivshar, Y. S. Nonlinear suppression of time reversals in PT-symmetric optical couplers. *Phys. Rev. A* **82**, 043818 (2010).
- Kang, M. S., Butsch, A. & Russell, P. St. J. Reconfigurable light-driven opto-acoustic isolators in photonic crystal fibre. *Nature Photon.* **5**, 549–553 (2011).
- Fan, L. *et al.* An all-silicon passive optical diode. *Science* **335**, 447–450 (2012).
- Armani, D. K., Kippenberg, T. J., Spillane, S. M. & Vahala, K. J. Ultra-high-Q toroid microcavity on a chip. *Nature* **421**, 925–928 (2003).
- Anetsberger, G. *et al.* Near-field cavity optomechanics with nanomechanical oscillators. *Nature Phys.* **5**, 904–914 (2009).
- Zheng, C. *et al.* Controllable optical analog to electromagnetically induced transparency in coupled high-Q microtoroid cavities. *Opt. Express* **20**, 18319–18325 (2012).
- Yang, L., Carmon, T., Min, B., Spillane, S. M. & Vahala, K. J. Erbium-doped and Raman microlasers on a silicon chip fabricated by the sol–gel process. *Appl. Phys. Lett.* **86**, 091114 (2005).
- Fan, H., Hua, S., Jiang, X. & Xiao, M. Demonstration of an erbium-doped microsphere laser on a silicon chip. *Laser Phys. Lett.* **10**, 105809 (2013).
- Mostafazadeh, A. Spectral singularities of complex scattering potentials and infinite reflection and transmission coefficients at real energies. *Phys. Rev. Lett.* **102**, 220402 (2009).
- Weiss, D. S. *et al.* Splitting of high-Q Mie modes induced by light backscattering in silica microspheres. *Opt. Lett.* **20**, 1835–1837 (1995).
- Kippenberg, T. J., Spillane, S. M. & Vahala, K. J. Modal coupling in traveling-wave resonators. *Opt. Lett.* **27**, 1669–1671 (2002).
- Grigoriev, V. & Biancalana, F. Nonreciprocal switching thresholds in coupled nonlinear microcavities. *Opt. Lett.* **36**, 2131–2133 (2011).
- Peng, B. *et al.* Parity–time-symmetric whispering-gallery microcavities. *Nature Phys.* **10**, 394–398 (2014).
- Carmon, T., Yang, L., & Vahala, K. J. Dynamical thermal behavior and thermal self-stability of microcavities. *Opt. Express* **12**, 4742–4750 (2004).

## Acknowledgements

This research was supported by the National Basic Research Program of China (nos. 2012CB921804 and 2011CBA00205), the National Natural Science Foundation of China (nos. 11104137 and 11321063), the Natural Science Foundation of Jiangsu Province, China (BK2011554) and the Specialized Research Fund for the Doctoral Program of Higher Education (20110091120015). J.M.W. and L.J. acknowledge funding support from a DARPA QUINNESS grant, the Alfred P. Sloan Foundation and the David and Lucile Packard Foundation. The authors thank Huibo Fan and Yang Ding for the preparation of the erbium-doped silica sol–gel film.

## Author contributions

X.J., J.W., L.J. and M.X. conceived the idea. X.J. and M.X. supervised the experiment with contributions from L.C., S.H., C.Y., G.L. and G.W. All authors contributed to the discussions about the project, analysis of experimental data and writing of the manuscript.

## Additional information

Supplementary information is available in the online version of the paper. Reprints and permissions information is available online at [www.nature.com/reprints](http://www.nature.com/reprints). Correspondence and requests for materials should be addressed to X.J., J.W. and M.X.

## Competing financial interests

The authors declare no competing financial interests.